analytical chemistry

pubs.acs.org/ac Article

Hydrazine Hydrate and Dissolved Oxygen-Triggered Near-Infrared Chemiluminescence from $CuInS_2$@ZnS Nanocrystals for Bioassays

Zhipeng Li, Xunxun Deng, Shuo Wu,* Shuangtian Dong, and Guizheng Zou*

Cite This: *Anal. Chem.* 2021, 93, 8931−8936 Read Online

ACCESS | Metrics & More | Article Recommendations | Supporting Information

ABSTRACT: The overwhelming majority of commercially available chemiluminescence (CL) assays are conducted in the eye-visible region. Herein, a near-infrared (NIR) aqueous CL strategy was proposed with $CuInS_2$@ZnS nanocrystals (CIS@ZnS NCs) as emitters. Hydrazine hydrate ($N_2H_4{\cdot}H_2O$) could inject electrons into the conduction band of the CIS@ZnS NCs and simultaneously transformed to the intermediate radical $N_2H_3^{\bullet}$. $N_2H_3^{\bullet}$ reduced dissolved oxygen (O_2) to $O_2^{-\bullet}$, while the $O_2^{-\bullet}$ could inject holes into the valence band of the CIS@ZnS NCs. The recombination of electrons and holes at Cu^+ defects in CIS@ZnS NCs eventually yielded efficient NIR CL at around 824.1 nm, which is the longest waveband for NCs CL to the best of our knowledge. The NIR CL could be conveniently performed in the neutral aqueous medium (pH 7.0) with a quantum yield of 0.0155 Einstein/mol and was successfully employed for constructing a signal-off CL biosensor with ascorbic acid as the analyte as well as a signal-on CL biosensor for determining ascorbate oxidase, which indicates that this NIR CL system has a promising potential for bioassays in diverse ways.

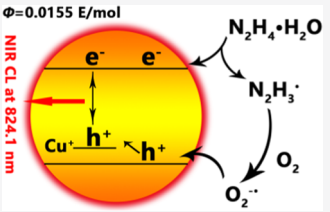

Chemiluminescence (CL) is a kind of optical radiation phenomenon driven by chemical reactions and has the merits of excellent signal-to-noise ratio, high sensitivity, and simple equipment because it eliminates the excitation light source. CL has been widely used in biosensors and commercialized immunodiagnosis.[1−3] Multicomponent detection in a single assay is attractive in bioanalysis for high-throughput detection and precise diagnosis.[4,5] Multicolor CL is more convenient to achieve this goal.[6] However, most commercial CL emitters glow in the visible region, and their emission wavebands normally overlap with each other.[1,6,7] Near-infrared (NIR, normally beyond 780 nm) CL is strongly anticipated to overwhelm this question. NIR CL was normally explored with conjugate-structured organic chemicals as emitters, and the emission waveband of the direct CL from these organic chemicals was limited to 780 nm.[8−10]

Nanocrystals (NCs) are usually employed as catalysts to enhance the CL intensity. For example, cobalt/gold bimetallic nanoclusters and oxidized g-C_3N_4 nanosheets act as catalysts of hydrogen peroxide to enhance the CL of luminol.[11,12] Recent investigations have demonstrated that NCs can also be directly employed as CL emitters, such as carbon dots,[13] CdTe,[14] black phosphorus quantum dots,[15] perovskite nanocrystal,[16] and so on.[17−19] Unfortunately, these CL with NCs as emitters, named NCs CL, were also mainly located within eye-visible wavebands, and the corresponding CL quantum yield (Φ_{CL}) was too low to be qualified for bioapplication.[20,21]

$CuInS_2$@ZnS NCs (CIS@ZnS NCs) are promising non-toxic-element NCs and have been adopted in photovoltaic cells and photoluminescence (PL).[22,23] Recently, investigations on electrogenerated CL (ECL) of CIS@ZnS NCs have provided unambiguous evidence that CIS@ZnS NCs are promising candidates for CL due to the interlinkage between CL and ECL.[24,25] Herein, we achieved efficient NIR CL from DL-lipoic acid (LA) and trisodium citrate (TSC)-capped CIS@ZnS NCs and proved that hydrazine hydrate ($N_2H_4{\cdot}H_2O$) cooperated with oxygen (O_2) to participate in the CL process. $N_2H_4{\cdot}H_2O$ injected electrons into the conduction band (CB) of CIS@ZnS NCs and was oxidized to $N_2H_3^{\bullet}$, while $N_2H_3^{\bullet}$ activated O_2 to $O_2^{-\bullet}$ and later injected holes into the valence band (VB) of CIS@ZnS NCs. The electrons and holes recombined at Cu^+ defects in CIS@ZnS NCs to emit NIR CL at 824.1 nm. The Φ_{CL} of CIS@ZnS NCs was 0.0155 Einstein/mol (E/mol), which is the highest value among the ever reported Φ_{CL} of NCs-based CL to the best of our knowledge. Furthermore, the proposed NIR CL can be conveniently performed in the neutral aqueous medium (pH 7.0). As the sensing applications of traditional CL systems are normally performed under strong alkaline conditions, CIS@ZnS NC-based NIR CL systems might be more favorable for CL bioassays.

EXPERIMENTAL SECTION

Chemicals and Materials. All reagents were of analytical grade and were used without further purification. Ultrapure water (resistivity, 18.25 MΩ·cm) was used throughout the experiments. Indium chloride tetrahydrate ($InCl_3{\cdot}4H_2O$),

Received: March 31, 2021
Accepted: June 7, 2021
Published: June 17, 2021

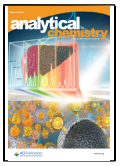

https://doi.org/10.1021/acs.analchem.1c01380
Anal. Chem. 2021, 93, 8931−8936

sodium sulfide (Na_2S), glutathione (reduced, GSH), tris-(hydroxymethyl)aminomethane (Tris), luminol, ammonium persulfate ($(NH_4)_2S_2O_8$), potassium iodate (KIO_3), ascorbic acid (AA), sodium thiosulfate ($Na_2S_2O_3$), hydroxylammonium chloride (NH_2OH), L-histidine, superoxide dismutase from bovine erythrocytes (SOD), glucose (Glu), bovine serum albumin (BSA), sodium chloride (NaCl), ammonium chloride (NH_4Cl), magnesium chloride ($MgCl_2$), potassium chloride (KCl), potassium carbonate (K_2CO_3), hemin, 2-morpholinoethanesulfonic acid (MES), 2-[4-(2-hydroxyethyl)piperazin-1-yl]ethanesulfonic acid (HEPES), ascorbate oxidase (AAO), and DL-lipoic acid (LA) were purchased from Aladdin. Potassium nitrate (KNO_3), copper chloride dihydrate ($CuCl_2{\cdot}2H_2O$), trisodium citrate dihydrate ($C_6H_3Na_3O_7{\cdot}2H_2O$, TSC), isopropyl alcohol (C_3H_8O), hydrogen peroxide (H_2O_2), potassium dichromate ($K_2Cr_2O_7$), hydrochloric acid (HCl), sodium hydroxide (NaOH), sodium hypochlorite (NaClO), dipotassium hydrogen phosphate trihydrate ($K_2PO_4{\cdot}3H_2O$, PB), and hydrazine hydrate solution ($N_2H_4{\cdot}H_2O$) were all of the analytical grade and purchased from Sinopharm Chemical Reagent Co., Ltd. (Shanghai, China). Thiourea and zinc acetate dihydrate ($Zn(CH_3COO)_2{\cdot}2H_2O$) were of analytical grade and were purchased from Guangcheng Chemical Reagent Co., Ltd. (Tianjin, China). Human serum samples were provided by volunteers from local hospitals.

Apparatus. The ultraviolet−visible (UV−vis) absorption spectrum was recorded on a TU-1901 spectrophotometer (Beijing Purkinje General Instrument Co., Ltd., China). The photoluminescence (PL) spectrum was recorded using an F-320 spectrofluorimeter (Tianjin Gangdong Sci. & Tech. Development Co., Ltd., China). The PL lifetime was recorded on an FLS920 fluorescence spectrometer (Edinburgh Instruments, U.K.). The X-ray diffraction (XRD) pattern was recorded using an X-ray diffractometer (Bruker AXS D8 Advance, Germany) with Cu Kα radiation (λ = 1.5418 Å). The high-resolution transmission electron microscopy (HRTEM) image was taken on a JEM 2100FS transmission electron microscope with an intermediate acceleration voltage of 200 kV (JEOL, Tokyo, Japan). X-ray photoelectron spectroscopy (XPS) was performed on an ESCALAB 250 XPS using monochromatic Al Kα radiation (Thermo Fisher Scientific Co.). CL curves were conducted on an MPI-II ECL analyzer (Xi'an Remex Analytical Instrument Co., Ltd., China) with PMT (H10721-20, Hamamatsu Photonics K.K., Japan, 230−920 nm) as the detector. CL spectra were obtained on a homemade spectrum analyzer consisting of an IsoPlane160 monochromator, a thermal electricity-cooled Pixis400BR CCD detector (Princeton Instruments). Fourier transform infrared spectra (FTIR) were recorded on a Fourier transform infrared spectrometer (Tensor II, Bruker). Electron spin resonance (ESR) was measured on an electron spin resonance spectrometer (JES-X320, JEOL). Cyclic voltammetry (CV) was conducted on a CHI 822 electrochemical workstation (CH Instrument) with a glassy carbon electrode (GCE) as the working electrode, a Ag/AgCl (saturated KCl) electrode as the reference electrode, and Pt coils as the counter electrode.

Preparation of LA and TSC-Capped CIS@ZnS NCs. The LA- and TSC-capped CIS@ZnS NCs were prepared according to the previously reported literature.[26] LA (0.2 mmol), NaOH (0.1 mmol), TSC (0.08 mmol), $CuCl_2$ (0.01 mmol), $InCl_3$ (0.04 mmol), and Na_2S (0.062 mmol) were added successively to 20 mL of water with continuous stirring. The reaction mixture was heated to 95 °C for 40 min, and then 1 mL of ZnS shell stock solution (pH 5.7) containing 0.08 mmol of $Zn(CH_3COO)_2$ and 0.08 mmol of thiourea was introduced into the solution for another 45 min at 95 °C. The crude CIS@ZnS NC was precipitated with isopropyl alcohol, purified via centrifugation several times, and then redispersed in ultrapure water. The concentration of CIS@ZnS NCs utilized for CL characterization was determined to be 3.0 μM according to the corresponding UV−vis spectrum (Figure S1) and the literature.[27]

The CIS@ZnS NCs-modified GCE, i.e., GCE|CIS@ZnS was prepared by dropping a drop of 10 μL of purified CIS@ZnS NCs onto the GCE surface and drying it under ambient conditions.

CL Measurement and Procedure for AA and AAO Detection. For CL measurement, the CIS@ZnS NCs solution was mixed with 1 mL of Tris−HCl buffer containing $N_2H_4{\cdot}H_2O$ at room temperature. Typically, the concentrations of CIS@ZnS NCs and $N_2H_4{\cdot}H_2O$ were 3.0 μM and 10 mM, respectively, and the pH was 7.0. The CL was recorded within 100 s, and the PMT was biased at −800 V. The CL spectra were collected on a homemade spectrum analyzer with an optical slit of 1.5 mm.

For AA detection, a drop of 30 μL of AA was injected into the CIS@ZnS NC solution and then mixed with 1 mL of Tris−HCl buffer containing $N_2H_4{\cdot}H_2O$ for CL measurements. Serum was employed for real sample detection. After the serum was centrifuged in an ultrafiltration tube (Millipore, 30 kDa), a drop of 30 μL of the filtrate was collected for AA CL determination. In the recovery experiments, AA of a specific concentration was added into the serum, and then the mixture was processed for CL measurements.

For AAO detection, a drop of 30 μL of AA (800 μM) was mixed with a drop of 30 μL of AAO, and then the mixture was incubated at 37 °C for 25 min. The obtained solution was injected into the CIS@ZnS NCs solution and then further mixed with 1 mL of Tris−HCl buffer containing $N_2H_4{\cdot}H_2O$ for the CL measurement.

RESULTS AND DISCUSSION

CL Performance of CIS@ZnS NCs. As shown in Figure 1A, the water-soluble CIS@ZnS NCs exhibited efficient CL and displayed a typical CL kinetic profile upon the addition of $N_2H_4{\cdot}H_2O$ with an initial rapid increase in signal to the maximum followed by a decrease.[28] The decay curve attenuated to the baseline was shown in Figure S2. The PL spectrum (Figure 1B) of CIS@ZnS NCs showed a major peak at 711.6 nm with a shoulder at 816.8 nm. This always occurred at quantum dots for a defect-related emission.[29,30] The corresponding PL decay curve of CIS@ZnS NCs (Figure S3) showed three order exponential decay, 34.72, 165.25, and 505.82 ns. Therefore, it was reasonable to attribute the emission at 816.8 nm to the defects in CIS@ZnS NCs. The CL spectrum of CIS@ZnS NCs in the presence of $N_2H_4{\cdot}H_2O$ (Figure 1B) showed the maximal emissions at 824.1 nm, which was the longest waveband for NCs-based CL to the best of our knowledge and different from commercial CL emitters that were mainly in the eye-visible region.[1,6,31] The peak of the CL spectrum was very close to 816.8 nm, so it could be inferred that the CL of CIS@ZnS NCs with $N_2H_4{\cdot}H_2O$ was defect-involved radiative-charge-transfer processes. The Φ_{CL} was defined as the relation between the number of photons emitted by a certain chemical reaction, per number of moles of the limiting reactant,[20] and the Φ_{CL} of CIS@ZnS NCs was

https://doi.org/10.1021/acs.analchem.1c01380
Anal. Chem. 2021, 93, 8931−8936

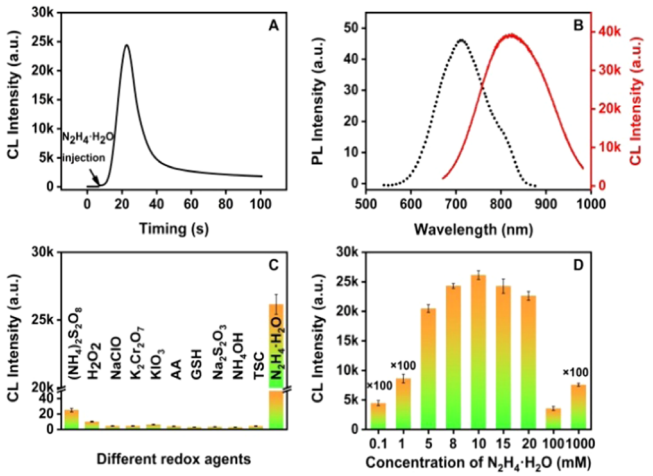

Figure 1. (A) CL intensity−time curve of CIS@ZnS NCs in 0.1 M Tris-HCl (pH 7.0) before and after the injection of 10 mM $N_2H_4·H_2O$; (B) PL of CIS@ZnS NCs (black line) and the CL spectrum of CIS@ZnS NCs in 0.1 M Tris−HCl (pH 7.0) containing 10 mM $N_2H_4·H_2O$ (red line); (C) CL intensity of CIS@ZnS NCs in 0.1 M Tris−HCl (pH 7.0) containing 10 mM different redox agents; and (D) effects of the $N_2H_4·H_2O$ concentration on the CL intensity of CIS@ZnS NCs in 0.1 M Tris−HCl (pH 7.0).

determined to be 0.0155 E/mol (luminol as the reference, Figure S2),[20] the highest value for the Φ_{CL} of NCs CL and higher than the reported Schapp's adamantylidene-dioxetane-based NIR CL (Table S1).[8,10,21,32] Different redox agents (Figure 1C) were also investigated to demonstrate their effects on the CL, and only $N_2H_4·H_2O$ could produce efficient CL. Although $(NH_4)_2S_2O_8$ and H_2O_2 could achieve CL to some extent, the luminous intensity was too weak to be practical. According to Figure 1D, 10 mM was chosen as the optimal concentration for $N_2H_4·H_2O$.

Effects of the CL Reaction on the Properties of CIS@ZnS NCs. The CIS@ZnS NCs showed three major XRD peaks (Figure 2A) at 27.765, 47.109, and 54.698°. Compared with CIS (PDF: 85-1575), they moved slightly toward ZnS (PDF: 05-0566). This phenomenon can also be observed in other nanomaterials with core−shell structures.[33] The crystal structure of CIS was chalcopyrite, features low band gap energy, broad emission, and an abundance of intrinsic defects due to the different bond lengths ($R_{Cu-S} \neq R_{In-S}$), causing anion displacement from a close-packed arrangement, leading to a tetragonal distortion of the crystal lattice.[34] It was in good agreement with its obvious defect emission in PL and CL spectra. The XRD pattern remained unchanged before and after CIS@ZnS NCs reacted with $N_2H_4·H_2O$, which proved that the structure of the nanoparticles was preserved during the CL reaction. TEM results (Figure S4) showed that the size of the NCs was also primarily preserved after the CL reaction. The FTIR spectra (Figure 2B) of CIS@ZnS NCs displayed different features. The band at 3433 cm^{-1} was typical oxygen−hydrogen (O−H) stretching vibration absorption bands, and 1619 and 1383 cm^{-1} corresponded to the carbonyl group (C═O).[22] After the CL reaction, a new absorption band appeared at 1015 cm^{-1}, which was similar to the symmetric stretching vibration of S═O in SO_3^-.[35−37] This meant that the LA ligands on the NC surface were oxidized during the CL process. XPS also revealed the occurrence of oxidation. The content of the oxygen element (Table S2) obviously increased, and other elements such as Cu, In, Zn, and S basically remained unchanged. Although Cu was easily oxidized, especially in a solution, there was no change in the valence state of Cu. Characters of Cu(I) were 932.3 and 952.3 eV with a splitting of 20 eV (Figure 2C). The oxidation of S was further confirmed by the new peak at 167.7 eV (S═O).[13,38] Since $N_2H_4·H_2O$ could only be used as a reducing agent,[39,40] and no other oxidants were added during the CL process, it could be inferred that dissolved oxygen (O_2) might participate in the reaction.

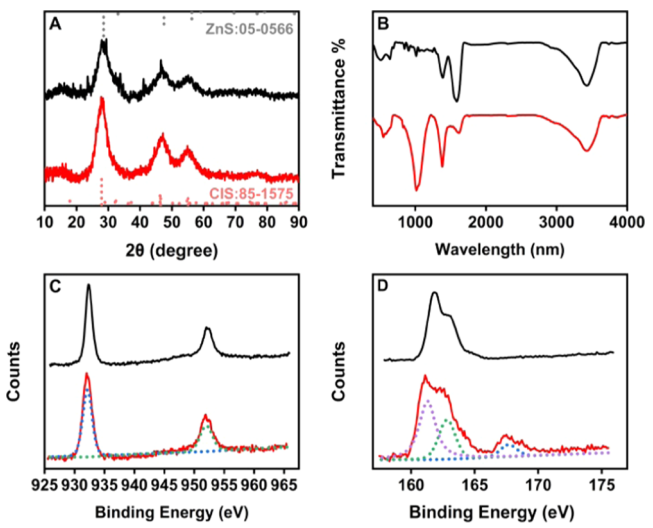

Figure 2. (A) XRD, (B) FTIR, (C) XPS spectra of element Cu, and (D) XPS spectra of element S. Black lines: CIS@ZnS NCs, red lines: product after CIS@ZnS NCs reacted with 10 mM $N_2H_4·H_2O$ in 0.1 M Tris−HCl (pH 7.0).

CL Mechanism. Control experiments were conducted to verify the role of O_2 in this CL system. First, CL performance (Figure 3A) was recorded after 10 min of nitrogen degassing. The CL intensity was decreased to 0.35 times that before deoxygenation for 10 min. Similar results were also observed in the ECL nature of CIS@ZnS NCs in which the electrons were injected via electrochemical reduction (Figure S5). There was no doubt that O_2 did participate in both the pure CL and the ECL processes and might act as an oxidant for injecting holes onto the VB of CIS@ZnS NCs. It can be concluded that $N_2H_4·H_2O$ was cooperated with O_2 to participate in the CL process. To further demonstrate the detailed chemical species for oxygen involved in the CL, three free radicals related to O_2, $OH^•$, $^1O_2$, and $O_2^{•-}$ were tested by radical scavengers. As shown in Figure 3B, thiourea (an effective scavenger of $OH^•$)[41] did not have any impact on the CL intensity, and histidine (an effective scavenger of $^1O_2$) merely slightly quenched the CL intensity. However, superoxide dismutase (SOD, an effective scavenger of $O_2^{•-}$)[42] completely inhibited the CL intensity, which further clarified that $O_2^{•-}$ was essential for the NIR CL emission. ESR was the most direct evidence to identify radicals. Only the spin adduct formed by 5,5-dimethyl-1-pyrroline-*N*-oxide (DMPO) and $O_2^{•-}$ (Figure 3C) could be detected when CIS@ZnS NCs and $N_2H_4·H_2O$ coexisted,[43] indicating that the coexisted CIS@ZnS NCs and O_2 were necessary for the generation of $O_2^{•-}$ radicals. CV was used to determine the redox characteristics of CIS@ZnS NCs via physically surface confining the CIS@ZnS NCs onto GCE (Figure 3D). Two oxidation peaks were observed at 0.685 V (Ox_1) and 1.155 V (Ox_2) with onset potentials of 0.488 and

https://doi.org/10.1021/acs.analchem.1c01380
Anal. Chem. 2021, 93, 8931−8936

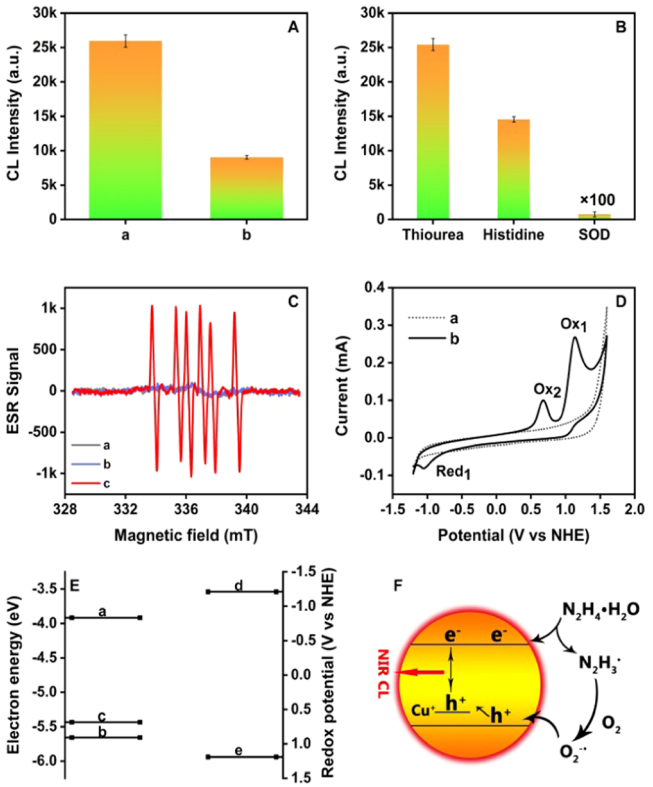

Figure 3. (A) CL intensity of CIS@ZnS NCs in 0.1 M Tris−HCl (pH 7.0) containing 10 mM $N_2H_4{\cdot}H_2O$ (a) before and (b) after deoxygenation; (B) effects of different free radical quenchers on the CL intensity of CIS@ZnS NCs in 0.1 M Tris−HCl (pH 7.0) containing 10 mM $N_2H_4{\cdot}H_2O$ and 10 mM thiourea, 10 mM histidine, or 1 mg/mL SOD; (C) ESR of (a) 20 mM DMPO + CIS@ZnS NCs, (b) $N_2H_4{\cdot}H_2O$, and (c) CIS@ZnS NCs—$N_2H_4{\cdot}H_2O$ in 0.1 M Tris−HCl (pH 7.0); (D) CV of (a) bare GCE and (b) GCE|CIS@ZnS in 0.1 M Tris-HCl (pH 7.0) containing 0.1 M KCl at 100 mV/s; (E) the energies for LUMO (a), HOMO (b), and Cu^+ defects (c) orbitals of CIS@ZnS NCs and the standard redox potentials of $N_2H_4{\cdot}H_2O$ (d) and $O_2^{\bullet-}$ (e); and (F) scheme of CL of CIS@ZnS NCs.

0.908 V, respectively, which were ascribed to the Cu^+ defects and the highest occupied molecular orbitals (HOMO). A reduction peak appeared at −1.055 V with an onset potential of −0.832 V (Red_1), which was attributed to the lowest unoccupied molecular orbital (LUMO) of CIS@ZnS NCs.[44,45] The Cu^+ defects, HOMO and LUMO energy levels were calculated to be −5.435, −5.658, and −3.918 eV, respectively (4.75 eV for 0.0 V vs NHE).[46] The difference between each two of them matched well with the results from the PL and CL spectral data of CIS@ZnS NCs, which were calculated according to the formula $E_g = 1240/\lambda$.[47,48] The standard oxidation potential of $N_2H_4{\cdot}H_2O$ and the reduction potential of $O_2^{-\bullet}$ were at −1.21 and 1.19 V, respectively,[49,50] allowing efficient electrons transferred from $N_2H_4{\cdot}H_2O$ to LUMO of CIS@ZnS NCs and holes from $O_2^{-\bullet}$ to HOMO of CIS@ZnS NCs (Figure 3E). It had been reported that $O_2^{\bullet-}$ could be generated from $N_2H_3^{\bullet}$ and O_2,[51] and the CL mechanism of CIS@ZnS NCs with $N_2H_4{\cdot}H_2O$ could be explained as follows: $N_2H_4{\cdot}H_2O$ acted as a reducing agent to inject electrons into the conduction band of CIS@ZnS NCs and formed $N_2H_3^{\bullet}$. Subsequently, $N_2H_3^{\bullet}$ reacted with O_2 to form $O_2^{\bullet-}$, which injected holes into the valence band of CIS@ZnS NCs. Then, the electrons and holes recombined and emitted light through the Cu^+ defects in CIS@ZnS NCs,[52] similar to the charge-transfer route for ECL of the CIS@ZnS NCs/$N_2H_4{\cdot}H_2O$ system.[53] Meanwhile, the surface ligand LA was simultaneously oxidized. This process was like CIS@ZnS NCs as a medium that bridged $N_2H_4{\cdot}H_2O$ and O_2. The scheme of the CL process is shown in Figure 3F.

CL Sensor for AA Detection. pH is crucial for free radical reactions and biosensors. The CL intensity (Figure 4A)

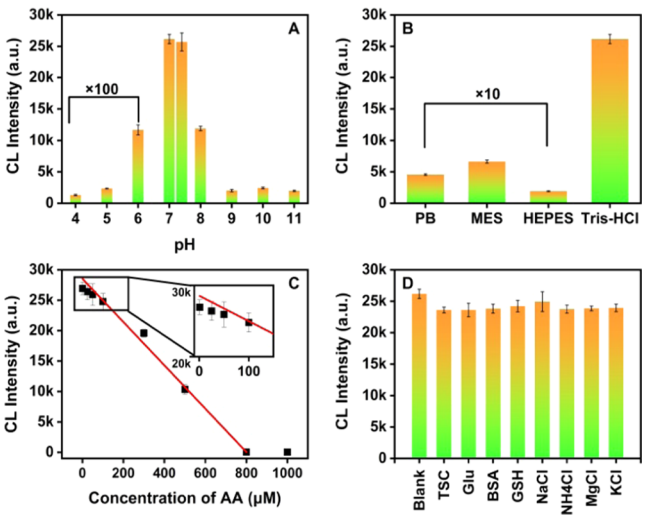

Figure 4. (A) Effects of pH on the CL intensity of CIS@ZnS NCs in 0.1 M Tris−HCl containing 10 mM $N_2H_4{\cdot}H_2O$; (B) effects of buffers on the CL intensity of CIS@ZnS NCs. The concentration of buffers was fixed at 0.1 M and pH of 7.0; (C) calibration curve for AA detection; and (D) CL intensity of the proposed NIR CL sensor toward samples containing 10% BSA as well as 10 mM TSC, Glu, GSH, NaCl, NH_4Cl, MgCl, and KCl, respectively. Inset of C: CL intensity with 1, 25, 50, 100 μM AA.

reached a maximum under neutral conditions (pH at 7.0). The NIR CL of CIS@ZnS NCs was consequently performed under neutral conditions, which was superior to the eye-visible CL of luminol/H_2O_2 and lucigenin/H_2O_2 performed under strong alkaline conditions.[54−56] According to Figure 4B, Tris−HCl buffer was chosen as the optimal buffer for the NIR CL of CIS@ZnS NCs. Since the NIR CL from CIS@ZnS NCs could be carried out under neutral conditions, AA was chosen as the model analyte to verify its biosensing potential, as the shortage and excessive intake of AA would result in many diseases, including scurvy, stomach, and so on. Figure 4C showed that the CL intensity decreased gradually with the increasing AA concentration. The linear range of AA for the NIR CL assay was 1−800 μM with the linear equations $I = -35.62\,[AA] + 28\,549$ ($R^2 = 0.9959$). The limit of detection was 0.3 μM (S/N = 3). The selectivity of the proposed signal-off NIR CL sensor for determining AA was also verified with the sample containing interfering substances, including 10% BSA as well as TSC, GSH, Glu, NaCl, KCl, MgCl, and NH_4Cl of 10 mM, respectively (Figure 4D). These interfering substances failed to exhibit any obvious influence on the CL intensity. Human serum was also used to evaluate the performance of the signal-off NIR CL sensor in actual samples. The concentration of AA in the serum was estimated to be 57.5 μM, which was consistent with previously reported results.[57] The recovery in human serum was 97.4−102% with the RSD smaller than 5% (n = 3) (Table 1). Importantly, as the CL of the proposed

https://doi.org/10.1021/acs.analchem.1c01380
Anal. Chem. 2021, 93, 8931−8936

Table 1. Recovery of the Proposed NIR CL Sensor for Detecting AA in Human Serum

added (μM)	founded (μM)	recovery (%)	RSD (%)
30	88.1	102	0.56
50	106.2	97.4	0.38
150	210.4	101.9	0.30

signal-off NIR CL sensor could be completely quenched with 800 μM AA, a signal-on NIR CL biosensor was further proposed to detect AAO by catalyzing the oxidation of 800 μM AA with AAO.[58] The linear range for determining AAO was 1−75 mU/mL, and the linear equation was $I/I_0 = 0.04$ [AAO] + 0.98 ($R^2 = 0.9992$, Figure S6 and Table S3). These results indicate that the NIR CL from CIS@ZnS NCs can be diversely utilized for biosensing.

CONCLUSIONS

In summary, an effective NIR CL strategy was proposed by employing CIS@ZnS NCs as emitters with the help of $N_2H_4{\cdot}H_2O$ and O_2. The detailed charge-transfer characterization proved that O_2 participated in the NIR CL reactions between CIS@ZnS NCs and $N_2H_4{\cdot}H_2O$ via the formation of $O_2^{-\bullet}$ radicals. Compared with the eye-visible CL of traditional luminol/H_2O_2 and lucigenin/H_2O_2 systems, which are normally performed under strong alkaline conditions, the NIR CL of CIS@ZnS NCs can be conveniently performed under neutral conditions with Φ_{CL} up to 0.0155 E/mol. The NIR CL from CIS@ZnS NCs can not only be utilized for determining AA in a signal-off way but also be employed to detect AAO in a signal-on way, indicating that the proposed NIR CL strategy is promising for NIR CL biosensing in diverse ways.

ASSOCIATED CONTENT

Supporting Information

The Supporting Information is available free of charge at https://pubs.acs.org/doi/10.1021/acs.analchem.1c01380.

Procedure, method, and UV−vis absorption employed for determining the concentration of CIS@ZnS NCs; CL intensity−time profiles, the spectral response of the PMT, and the method employed for determining Φ_{CL}; PL lifetime of CIS@ZnS NCs; effects of the CL reaction on TEM, HRTEM, and elemental content of CIS@ZnS NCs; effects of dissolved oxygen on ECL of CIS@ZnS NCs; CL properties of other CL emitters; and calibration curve for AAO detection and comparison of different methods for AA and AAO detection (PDF)

AUTHOR INFORMATION

Corresponding Authors

Shuo Wu − *School of Chemical Engineering, Dalian University of Technology, Dalian 116024, China;* orcid.org/0000-0003-1610-3875; Email: wushuo@dlut.edu.cn

Guizheng Zou − *School of Chemistry and Chemical Engineering, Shandong University, Jinan 250100, China;* orcid.org/0000-0002-3295-3848; Email: zouguizheng@sdu.edu.cn

Authors

Zhipeng Li − *School of Chemical Engineering, Dalian University of Technology, Dalian 116024, China; School of Chemistry and Chemical Engineering, Shandong University, Jinan 250100, China;* orcid.org/0000-0003-2642-1308

Xunxun Deng − *School of Chemical Engineering, Dalian University of Technology, Dalian 116024, China*

Shuangtian Dong − *School of Chemistry and Chemical Engineering, Shandong University, Jinan 250100, China;* orcid.org/0000-0002-5799-788X

Complete contact information is available at: https://pubs.acs.org/10.1021/acs.analchem.1c01380

Notes

The authors declare no competing financial interest.

ACKNOWLEDGMENTS

This project was supported by the National Natural Science Foundation of China (Grant nos. 21427808 and 21675018) and the Fundamental Research Funds of Shandong University (ZY202006).

REFERENCES

(1) Yang, M.; Huang, J.; Fan, J.; Du, J.; Pu, K.; Peng, X. *Chem. Soc. Rev.* **2020**, *49*, 6800−6815.
(2) Hai, Z.; Li, J.; Wu, J.; Xu, J.; Liang, G. *J. Am. Chem. Soc.* **2017**, *139*, 1041−1044.
(3) An, R.; Wei, S.; Huang, Z.; Liu, F.; Ye, D. *Anal. Chem.* **2019**, *91*, 13639−13646.
(4) Wang, X.; Zhang, Y.; Sun, L.; Wang, S.; Nie, J.; Zhao, W.; Zheng, G. *J. Clin. Lab. Anal.* **2018**, *32*, No. e22565.
(5) Liu, F.; Du, F.; Chen, X. *World J. Surg. Oncol.* **2014**, *12*, No. 333.
(6) Browne, K. A.; Deheyn, D. D.; El-Hiti, G. A.; Smith, K.; Weeks, I. *J. Am. Chem. Soc.* **2011**, *133*, 14637−14648.
(7) Mayer, A.; Neuenhofer, S. *Angew. Chem., Int. Ed.* **1994**, *33*, 1044−1072.
(8) Green, O.; Gnaim, S.; Blau, R.; Eldar-Boock, A.; Satchi-Fainaro, R.; Shabat, D. *J. Am. Chem. Soc.* **2017**, *139*, 13243−13248.
(9) Bruemmer, K. J.; Green, O.; Su, T. A.; Shabat, D.; Chang, C. J. *Angew. Chem., Int. Ed.* **2018**, *57*, 7508−7512.
(10) Huang, J.; Jiang, Y.; Li, J.; Huang, J.; Pu, K. *Angew. Chem., Int. Ed.* **2021**, *60*, 3999−4003.
(11) Gao, B.; Haghighatbin, M. A.; Cui, H. *Anal. Chem.* **2020**, *92*, 10677−10685.
(12) Sun, X.; Lei, J.; Jin, Y.; Li, B. *Anal. Chem.* **2020**, *92*, 11860−11868.
(13) Dong, S.; Yuan, Z.; Zhang, L.; Lin, Y.; Lu, C. *Anal. Chem.* **2017**, *89*, 12520−12526.
(14) Zhou, W.; Cao, Y.; Sui, D.; Lu, C. *Anal. Chem.* **2016**, *88*, 2659−2665.
(15) Liu, H.; Su, Y.; Deng, D.; Song, H.; Lv, Y. *Anal. Chem.* **2019**, *91*, 9174−9180.
(16) Fan, Y.; Xing, H.; Zhai, Q.; Fan, D.; Li, J.; Wang, E. *Anal. Chem.* **2018**, *90*, 11651−11657.
(17) Liu, J.; Chen, H.; Lin, Z.; Lin, J. *Anal. Chem.* **2010**, *82*, 7380−7386.
(18) Tang, Y.; Su, Y.; Yang, N.; Zhang, L.; Lv, Y. *Anal. Chem.* **2014**, *86*, 4528−4535.
(19) Chen, H.; Wang, Q.; Shen, Q.; Liu, X.; Li, W.; Nie, Z.; Yao, S. *Biosens. Bioelectron.* **2017**, *91*, 878−884.
(20) Augusto, F. A.; de Souza, G. A.; de Souza Junior, S. P.; Khalid, M.; Baader, W. J. *Photochem. Photobiol.* **2013**, *89*, 1299−1317.
(21) Cui, H.; Zhang, Z. F.; Shi, M. J.; Xu, Y.; Wu, Y. L. *Anal. Chem.* **2005**, *77*, 6402−6406.
(22) Liu, J.; Zhao, X.; Xu, H.; Wang, Z.; Dai, Z. *Anal. Chem.* **2019**, *91*, 8987−8993.
(23) Li, Z.-Q.; Mo, C.-J.; Guo, Y.; Xu, N.-N.; Zhu, Q.-Y.; Dai, J. *J. Mater. Chem. A* **2017**, *5*, 8519−8525.

(24) Fu, L.; Zhang, B.; Fu, K.; Gao, X.; Zou, G. *Anal. Chem.* **2020**, *92*, 6144−6149.
(25) Li, Z.; Wu, S.; Zhang, B.; Fu, L.; Zou, G. *J. Phys. Chem. Lett.* **2019**, *10*, 5408−5413.
(26) Chen, Y.; Li, S.; Huang, L.; Pan, D. *Inorg. Chem.* **2013**, *52*, 7819−7821.
(27) Booth, M.; Brown, A. P.; Evans, S. D.; Critchley, K. *Chem. Mater.* **2012**, *24*, 2064−2070.
(28) Roth-Konforti, M. E.; Bauer, C. R.; Shabat, D. *Angew. Chem., Int. Ed.* **2017**, *56*, 15633−15638.
(29) Liu, S.; Zhang, Q.; Zhang, L.; Gu, L.; Zou, G.; Bao, J.; Dai, Z. *J. Am. Chem. Soc.* **2016**, *138*, 1154−1157.
(30) Wang, F.; Lin, J.; Zhao, T.; Hu, D.; Wu, T.; Liu, Y. *J. Am. Chem. Soc.* **2016**, *138*, 7718−7724.
(31) Hananya, N.; Shabat, D. *ACS Cent. Sci.* **2019**, *5*, 949−959.
(32) Shen, C. L.; Lou, Q.; Lv, C. F.; Zang, J. H.; Qu, S. N.; Dong, L.; Shan, C. X. *Adv. Sci.* **2019**, *6*, No. 1802331.
(33) Li, J. J.; Wang, A. Y.; Guo, W. Z.; Keay, J. C.; Mishima, T. D.; Johnson, M. B.; Peng, X. G. *J. Am. Chem. Soc.* **2003**, *125*, 12567−12575.
(34) Leach, A. D.; Macdonald, J. E. *J. Phys. Chem. Lett.* **2016**, *7*, 572−583.
(35) Şahin, Y.; Pekmez, K.; Yıldız, A. *J. Appl. Polym. Sci.* **2003**, *90*, 2163−2169.
(36) Abdiryim, T.; Zhang, X. G.; Ruxangul, J. *J. Appl. Polym. Sci.* **2005**, *96*, 1630−1634.
(37) Warren, D. S.; McQuillan, A. J. *J. Phys. Chem. B* **2008**, *112*, 10535−10543.
(38) Moulder, J. F.; Stickle, W. F.; Sobol, P. E.; Bomen, K. D. *Handbook of X-ray Photoelectron Spectroscopy*; Perkin-Elmer: Eden Prairie, Minnesota, USA, 1992.
(39) Zhou, D.; Lin, M.; Chen, Z.; Sun, H.; Zhang, H.; Sun, H.; Yang, B. *Chem. Mater.* **2011**, *23*, 4857−4862.
(40) Liang, G.; Liu, S.; Zou, G.; Zhang, X. *Anal. Chem.* **2012**, *84*, 10645−10649.
(41) Wang, W.-F.; Schuchmann, M. N.; Schuchmann, H.-P.; Knolle, W.; Sonntag, J. V.; Sonntag, C. V. *J. Am. Chem. Soc.* **1999**, *121*, 238−245.
(42) Schaap, A. P.; Thayer, A. L.; Faler, G. R.; Goda, K.; Kimura, T. *J. Am. Chem. Soc.* **1974**, *96*, 4025−4026.
(43) Villamena, F. A.; Locigno, E. J.; Rockenbauer, A.; Hadad, C. M.; Zweier, J. *J. Phys. Chem. A* **2007**, *111*, 384−391.
(44) Nagamine, G.; Nunciaroni, H. B.; McDaniel, H.; Efros, A. L.; de Brito Cruz, C. H.; Padilha, L. A. *Nano Lett.* **2018**, *18*, 6353−6359.
(45) van der Stam, W.; de Graaf, M.; Gudjonsdottir, S.; Geuchies, J. J.; Dijkema, J. J.; Kirkwood, N.; Evers, W. H.; Longo, A.; Houtepen, A. J. *ACS Nano* **2018**, *12*, 11244−11253.
(46) Cardona, C. M.; Li, W.; Kaifer, A. E.; Stockdale, D.; Bazan, G. C. *Adv. Mater.* **2011**, *23*, 2367−2371.
(47) Guo, Y.; Liu, D.; Miao, C.; Sun, J.; Pang, Z.; Wang, P.; Xu, M.; Han, N.; Yang, Z.-X. *Nanotechnology* **2021**, *32*, No. 145203.
(48) Zhao, W.; Ribeiro, R. M.; Eda, G. *Acc. Chem. Res.* **2015**, *48*, 91−99.
(49) Granot, E.; Filanovsky, B.; Presman, I.; Kuras, I.; Patolsky, F. *J. Power Sources* **2012**, *204*, 116−121.
(50) Wood, P. M. *Biochem. J.* **1988**, *253*, 287−289.
(51) Buxton, G. V.; Sims, H. E. *Phys. Chem. Chem. Phys.* **2000**, *2*, 4941−4946.
(52) Long, X.; Tan, X.; He, Y.; Zou, G. *J. Mater. Chem. C* **2017**, *5*, 12393−12399.
(53) Fu, L.; Zhang, B.; Long, X. Y.; Fu, K. N.; Gao, X. W.; Zou, G. Z. *Anal. Chem.* **2019**, *91*, 10221−10226.
(54) Saqib, M.; Lou, B.; Halawa, M. I.; Kitte, S. A.; Liu, Z.; Xu, G. *Anal. Chem.* **2017**, *89*, 1863−1869.
(55) Kishikawa, N.; El-Maghrabey, M.; Nagamune, Y.; Nagai, K.; Ohyama, K.; Kuroda, N. *Anal. Chem.* **2020**, *92*, 6984−6992.
(56) Lan, Y.; Yuan, F.; Fereja, T. H.; Wang, C.; Lou, B.; Li, J.; Xu, G. *Anal. Chem.* **2019**, *91*, 2135−2139.
(57) Simon, J. A.; Hudes, E. S. *Arch. Intern. Med.* **2000**, *160*, 931−936.
(58) Zelinová, V.; Halušková, Ld.; Mistrík, I.; Tamás, L. *Plant Soil* **2011**, *349*, 281−289.

https://doi.org/10.1021/acs.analchem.1c01380
Anal. Chem. 2021, 93, 8931−8936